Journal of Radioanalytical and Nuclear Chemistry (2025) 334:953–967
https://doi.org/10.1007/s10967-024-09821-y

Prompt gamma rays of lanthanum and praseodymium produced by inelastic scattering of fission neutrons

Niklas Ophoven[1] · Eric Mauerhofer[1] · Zeljko Ilic[1,2] · Christian Stieghorst[3] · Zsolt Révay[3] · Iaroslav Meleshenkovskii[1] · Tsitohaina H. Randriamalala[1]

Received: 28 August 2024 / Accepted: 4 October 2024 / Published online: 19 October 2024

Abstract
Emission of prompt gamma rays in lanthanum and praseodymium nuclei triggered by (n,n'γ) inelastic scattering reactions of fission neutrons was investigated with the instrument FaNGaS (Fast Neutron-induced Gamma-ray Spectrometry) at Heinz Maier-Leibnitz Zentrum (MLZ). We identified 125 gamma lines (54 for lanthanum and 71 for praseodymium), for which we give the relative intensities and production cross sections. Presence of oxygen and chlorine in the samples was exploited to verify previous measurements. Our results are consistent with available literature data but also enhance it as we detect new lines and recognize a few false assignments. In addition, for a counting time of 12 h we estimated the detection limits of lanthanum and praseodymium as 0.6 and 0.4 mg, respectively.

Keywords Inelastic scattering · Lanthanum · Praseodymium · Chlorine · Oxygen · Cross section · Gamma ray

Introduction

The non-destructive elemental analysis of materials based on the detection of neutron-induced gamma radiation is a well-established and powerful tool in nuclear science and industry. The accuracy in mass quantification of this method requires precise knowledge on nuclear data, in particular gamma-ray production cross sections. In the case of Prompt Gamma Neutron Activation Analysis (PGNAA) [1], validated databases exist [2–4], that provide the aforementioned information. For Prompt Gamma Analysis based on Neutron Inelastic Scattering (PGAINS), however, only one larger set of data is available: the "Atlas of Gamma-rays from the Inelastic Scattering of Reactor Fast Neutrons", published by Demidov et al. in 1978 [5]. This "Demidov Atlas" contains peak energies and relative intensities of 7375 gamma rays for 105 different target materials (76 natural and 29 isotopically-enriched), measured with a Ge(Li) gamma-ray detector that was oriented at an angle of 90° with respect to the incident neutron beam axis. The emission of gamma rays was induced by a fast-neutron spectrum with a mean energy of about 0.6 MeV. For irradiation, the samples with masses between 1 and 125 g were contained in a 25×25 mm^2 holder and tilted by 60° relative to the incident neutron beam [5, 6]. Although the data listed in the Demidov Atlas is valuable and a relational database was built based on it [7], this work was never validated and gamma-ray production cross sections are missing. To address this gap in nuclear data for fast-neutron inelastic scattering and to provide enhanced nuclear data that meets the currently observed demand [8–10], the data listed in the Demidov Atlas is checked by measurements with the FaNGaS (Fast Neutron-Induced Gamma-ray Spectrometry) instrument [11–20] operated at MLZ (Heinz Maier-Leibnitz Zentrum) for chemical analysis. FaNGaS utilizes a beam of fission neutrons generated from an uranium (93% ^{235}U) converter plugged into the heavy water moderator of the research reactor FRM II (Forschungs-Neutronenquelle Heinz Maier-Leibnitz) and extracted through the beam tube SR10 into the irradiation room via a set of filters and collimators [12, 14, 21]. The gamma radiation generated by interactions of fast neutrons with the sample is measured with an electromechanically-cooled high-purity germanium

✉ Eric Mauerhofer
e.mauerhofer@fz-juelich.de

1 Jülich Centre for Neutron Science, Forschungszentrum Jülich GmbH, 52425 Jülich, Germany

2 Lehrstuhl Für Experimentalphysik IVc, RWTH Aachen University, 52056 Aachen, Germany

3 Heinz Maier-Leibnitz Zentrum (MLZ), Technische Universität München, Lichtenbergstraße 1, 85748 Garching, Germany

(HPGe) detector at an angle of 90° between neutron beam and detector. The measurements performed with FaNGaS enable the validatation of Demidov´s data on a relative scale on the one hand, but do also complement it on the other hand as the mean neutron energy of about 2.2 MeV is closer to the value of a fission spectrum. In our previous works we could demonstrate the necessity for a meticulous reevaluation of Demidov´s data [14–20].

In this work, we report on the nuclear data obtained from the measurement of the prompt gamma rays of lanthanum and praseodymium produced by inelastic scattering of fast neutrons on a lanthanum(III) chloride heptahydrate ($LaCl_3{\cdot}7H_2O$) and a praseodymium(III) chloride heptahydrate ($PrCl_3{\cdot}7H_2O$) sample, respectively. Relative intensities and fast-neutron spectrum-averaged partial cross sections of the identified gamma lines are compared, with available literature data. Additionally, cross sections measured for observed oxygen and chlorine lines are compared with the values previously obtained in [17–19]. Furthermore, we give the elemental detection limit for lanthanum and praseodymium.

Experimental

Prompt gamma radiation was produced by interaction of fission neutrons with a $LaCl_3{\cdot}7H_2O$ and a $PrCl_3{\cdot}7H_2O$ powder sample ($LaCl_3{\cdot}7H_2O$ mass: 1.51 g, La: 0.57 g, Cl: 0.43 g, O: 0.46 g; $PrCl_3{\cdot}7H_2O$ mass: 1.49 g, Pr: 0.56 g, Cl: 0.42 g, O: 0.45 g). It was investigated with the FaNGaS instrument [17, 19]. The powder was sealed into a small bag of PTFE (polytetrafluorethylene). The thickness was estimated as 4 mm for both aforementioned samples. The samples were fixed to a thin PTFE rod and tilted by an angle of 45° with respect to the neutron beam direction. At sample position, the fast-neutron flux was $(1.13 \pm 0.04) \times 10^8$ cm^{-2} s^{-1} (neutron-energy range: 0.06–20 MeV). The neutron flux (energy range: 10^{-10}–20 MeV) is given in Table 1 in the supplementary materials. The $LaCl_3{\cdot}7H_2O$ sample was irradiated for 13.1 h and the $PrCl_3{\cdot}7H_2O$ sample for 7.6 h. The samples were counted (live time) for 10.9 and 6.3 h, respectively. Perpendicular to the neutron beam direction, i.e. at an angle of 90°, the gamma rays were detected at a sample-to-detector distance of 67 cm. The HYPERMET-PC software [22] was used to analyze the recorded spectra, which are depicted in Figs. 1, 2, 3 and 4. Fast-neutron induced prompt gamma rays were identified using the NuDat 3.0 database [23] as well as related nuclear data from different evaluations for all nuclides covered in this work [24–30]. Identification of gamma rays from (n,γ) reactions was done with the PGNAA database [2].

As a certain part of neutrons scatters from the sample towards the detector the count rate of background lines was found to be increased by a mean factor of 1.44 ± 0.08 and 1.68 ± 0.18, respectively, for the $LaCl_3{\cdot}7H_2O$ and the $PrCl_3{\cdot}7H_2O$ sample. These factors were used in the interference corrections of background lines. Relevant interferences arising from single or double escape peaks were found in the $PrCl_3{\cdot}7H_2O$ spectrum and corrected with the curves given in [18].

Method

Given a prompt gamma ray of energy E_γ, which was produced by neutron capture or inelastic neutron scattering, the net peak area, i.e. $P_{E\gamma}$, can be generally described as [1, 14–20]:

$$P_{E\gamma} = \frac{m}{M} \cdot N_A \cdot h \cdot \varepsilon_{E\gamma} \cdot \langle \sigma_{E\gamma} \rangle \cdot \langle \Phi \rangle \cdot t_c \cdot f_n \cdot f_{\mathrm{mod}} \cdot f_{E\gamma} \quad (1)$$

where m (g) is the mass of the irradiated element, M (g mol^{-1}) the molar mass of the element, N_A the Avogadro number, h the abundance of the considered isotope, $\varepsilon_{E\gamma}$ the full-energy-peak (FEP) efficiency, $<\sigma_{E\gamma}>$ (cm^2) the spectrum-averaged isotopic cross section for gamma-ray production, $<\Phi>$ (cm^{-2} s^{-1}) the integral neutron flux in the energy range of interest, t_c (s) the counting (live) time, f_n accounts for neutron self-shielding and $f_{E\gamma}$ for gamma-ray self-absorption. Neutron moderation in water-containing samples is expressed through the factor f_{mod}.

The gamma-ray self-absorption factor $f_{E\gamma}$ was estimated with the following expression [1, 31]:

$$f_{E\gamma} = \frac{1 - e^{-\frac{\mu}{\rho} \cdot \rho \cdot l}}{\frac{\mu}{\rho} \cdot \rho \cdot l} \quad (2)$$

where $l = 0.57$ cm is the effective thickness of the samples, μ/ρ (cm^2 g^{-1}) represents the mass attenuation coefficient and $\rho = 2.23$ g cm^{-3} and $\rho = 2.25$ g cm^{-3} are the sample densities of the $LaCl_3{\cdot}7H_2O$ and the $PrCl_3{\cdot}7H_2O$ sample, respectively. The value of μ/ρ was gained from the database XCOM [32, 33], including coherent scattering. For several gamma-ray energies ranging between 100 and 5000 keV the corresponding $f_{E\gamma}$ values were calculated after Eq. (2). The dependence of the gamma-ray self-absorption factors $f_{E\gamma}$ on the gamma-ray energy E_γ is depicted in Figs. 5 and 6, respectively. The data points were fitted with the following semi-empirical function:

$$f = a_0 + a_1 \cdot \left(1 - e^{-a_2 \cdot E_\gamma}\right) + a_3 \cdot \left(1 - e^{-a_4 \cdot E_\gamma}\right) \quad (3)$$

with $a_0 = -1.4201 \pm 0.1571$, $a_1 = -2.2959 \pm 0.1499$, $a_2 = 0.0197 \pm 0.0008$, $a_3 = 1.008 \pm 0.0098$ and $a_4 = 0.0020 \pm 0.0003$ for the $LaCl_3{\cdot}7H_2O$, and with $a_0 = -1.4765 \pm 0.1432$, $a_1 = -0.1057 \pm 0.0104$,

Table 1 Prompt gamma rays of ^{139}La induced by inelastic scattering of fast neutrons

This work				From Demidov Atlas [5]		*R*
E_γ (keV)	$P_{E\gamma}$ (90°)/$(\varepsilon_{E\gamma} \cdot f_{E\gamma}) \times 10^{-8}$ (count)	I_R (relative) (%)	$<\sigma_{E\gamma}$ (90°)> (mb)	E_γ (keV)	I_R (relative) (%)	
97.11 ± 0.05	0.98 ± 0.06	11.0 ± 0.8	8.98 ± 0.63	–	–	–
153.43 ± 0.12[a]	0.29 ± 0.04	3.24 ± 0.48	2.65 ± 0.38	–	–	–
165.73 ± 0.04	63 ± 2	702 ± 31	574 ± 27	165.85 ± 10[b]	930 ± 150	− 1.49
174.44 ± 0.04[c]	2.28 ± 0.19	26 ± 2	21 ± 2	174.6 ± 0.2	20 ± 5	1.02
232.60 ± 0.06	0.73 ± 0.05	8.14 ± 0.60	6.65 ± 0.51	232.5 ± 0.6	9.1 ± 1.0	− 0.82
246.55 ± 0.08[a]	0.33 ± 0.03	3.73 ± 0.40	3.05 ± 0.30	–	–	–
290.83 ± 0.04	1.54 ± 0.07	17.3 ± 0.9	14.1 ± 0.81	291.3 ± 0.2	16.5 ± 1.5	0.43
307.92 ± 0.05	0.76 ± 0.05	8.55 ± 0.60	6.99 ± 0.52	308.3 ± 0.3	10.6 ± 1.5	− 1.27
330.14 ± 0.04[d]	4.52 ± 0.18	51 ± 3	41 ± 2	330.7 ± 0.1	54 ± 5	− 0.58
362.43 ± 0.10	0.58 ± 0.07	6.52 ± 0.81	5.33 ± 0.67	363.1 ± 0.2	8.9 ± 1.0	− 1.85
402.61 ± 0.07	1.08 ± 0.10	12.1 ± 1.2	9.86 ± 0.98	403.8 ± 0.2	9.8 ± 1.5	1.19
424.43 ± 0.05	1.77 ± 0.12	19.8 ± 1.4	16.2 ± 1.2	425.2 ± 0.2	20 ± 3	− 0.05
495.22 ± 0.12[d]	0.32 ± 0.06	3.56 ± 10.70	2.91 ± 0.55	–	–	–
579.35 ± 0.07	0.34 ± 0.04	3.86 ± 0.43	3.15 ± 0.38	581.3 ± 0.5	7 ± 2	− 1.53
1042.90 ± 0.07	1.82 ± 0.08	20 ± 1	16.7 ± 0.94	1043.1 ± 0.3	15 ± 4	1.30
1052.85 ± 0.08	0.74 ± 0.06	8.29 ± 0.71	6.77 ± 0.60	1054.2 ± 0.8	8 ± 3	0.09
1090.70 ± 0.06[c]	2.62 ± 0.34	29 ± 4	24 ± 3	1090.97 ± 10	33 ± 3	− 0.73
1215.50 ± 0.06	13.50 ± 0.44	151 ± 7	124 ± 6	1215.49 ± 10	137 ± 15	0.87
1219.24 ± 0.06	5.77 ± 0.72	65 ± 8	53 ± 7	1219.10 ± 10	80 ± 10	− 1.17
1242.78 ± 0.19[a]	0.30 ± 0.06	3.33 ± 0.65	2.72 ± 0.55	–	–	–
1254.12 ± 0.31	0.56 ± 0.10	6.29 ± 1.15	5.14 ± 0.93	–	–	–
1256.57 ± 0.14	1.47 ± 0.13	16.5 ± 1.6	13.5 ± 1.3	1256	25 ± 3[e]	− 0.40
1310.65 ± 0.07	4.60 ± 0.15	52 ± 2	42 ± 2	1310.64 ± 15	48 ± 5	0.65
1370.49 ± 0.08[d]	1.36 ± 0.07	15.3 ± 0.9	12.5 ± 0.8	1370.5 ± 0.2	16.6 ± 1.5	− 0.74
1381.38 ± 0.12	0.74 ± 0.06	8.26 ± 0.72	6.75 ± 0.60	1381.1 ± 0.2	6.6 ± 0.7	1.65
1392.84 ± 0.09[c]	0.77 ± 0.04	8.63 ± 0.57	7.06 ± 0.44	1392.4 ± 0.2	8.7 ± 0.8	− 0.07
1420.53 ± 0.07[c]	8.91 ± 0.28	100	82 ± 4	1420.56 ± 10	100	–
1476.28 ± 0.14	0.86 ± 0.07	9.64 ± 0.83	7.88 ± 0.70	1476.1 ± 0.4	6.6 ± 0.7	2.80
1537.86 ± 0.07	14.38 ± 0.44	161 ± 7	132 ± 6	1537.69 ± 10	144 ± 14	1.11
1558.33 ± 0.08[c]	1.13 ± 0.17	12.7 ± 2.0	10.3 ± 1.6	1558.5 ± 0.2	11.8 ± 1.2	0.37
1578.16 ± 0.07	6.85 ± 0.22	77 ± 3	63 ± 3	1578.09 ± 10	72 ± 7	0.61
1595.20 ± 0.13[c,d]	1.37 ± 0.11	15.4 ± 1.4	12.6 ± 1.1	1595.6	18 ± 3	− 0.80
1600.27 ± 0.14[c,d]	1.01 ± 0.06	11.3 ± 0.8	9.22 ± 0.64	1600.9 ± 0.6	10 ± 2	0.60
1625.55 ± 0.22[a,c,d]	0.23 ± 0.03	2.61 ± 0.35	2.13 ± 0.29	1626.7 ± 0.8	3.1 ± 0.4	− 0.92
1683.10 ± 0.08	2.99 ± 0.11	34 ± 2	27 ± 1	1683.1 ± 0.2	35 ± 4	− 0.34
1690.49 ± 0.13	0.74 ± 0.08	8.33 ± 0.89	6.80 ± 0.77	1690.6 ± 0.3	10.4 ± 1.5	− 1.19
1716.14 ± 0.09	3.72 ± 0.19	42 ± 2	34 ± 2	1716.11 ± 10	37 ± 4	1.00
1754.60 ± 0.11	0.80 ± 0.05	8.94 ± 0.59	7.30 ± 0.52	1755.0 ± 0.4	10.4 ± 1.2	− 1.09
1797.09 ± 0.11[c]	0.45 ± 0.03	5.03 ± 0.36	4.11 ± 0.31	1797.1 ± 0.4	7.1 ± 0.8	− 2.36
1853.68 ± 0.09	1.88 ± 0.08	21 ± 1	17.3 ± 0.9	1853.64 ± 10	22 ± 2	− 0.39
1894.28 ± 0.23	0.38 ± 0.05	4.28 ± 0.53	3.50 ± 0.48	1894.0	4.7 ± 0.6	− 0.52
1920.41 ± 0.10	1.10 ± 0.05	12.4 ± 0.6	10.1 ± 0.6	1920.7 ± 0.2	12.5 ± 1.5	− 0.09
2060.22 ± 0.14	0.50 ± 0.04	5.56 ± 0.49	4.54 ± 0.40	2060.9 ± 0.5	6.6 ± 0.8	− 1.11
2070.58 ± 0.32[a]	0.39 ± 0.05	4.43 ± 0.53	3.62 ± 0.48	2071.4 ± 0.6	3.7 ± 0.5	− 1.11
2087.60 ± 0.27[a]	0.37 ± 0.05	4.11 ± 0.55	3.36 ± 0.47	–	–	–
2209.63 ± 0.47[a,c]	0.24 ± 0.05	2.71 ± 0.58	2.22 ± 0.47	2210.5 ± 0.8	12 ± 2	− 4.46
2243.79 ± 0.16[a]	0.45 ± 0.04	5.01 ± 0.43	4.09 ± 0.39	2244.6 ± 1.0	2.8 ± 0.5	3.37

Table 1 (continued)

This work				From Demidov Atlas [5]		*R*
E_γ (keV)	$P_{E\gamma}$ (90°)/$(\varepsilon_{E\gamma} \cdot f_{E\gamma}) \times 10^{-8}$ (count)	I_R (relative) (%)	$<\sigma_{E\gamma}$ (90°)> (mb)	E_γ (keV)	I_R (relative) (%)	
2275.87 ± 0.28[c]	0.26 ± 0.08	2.88 ± 0.89	2.36 ± 0.73	2276.2 ± 1.2	4.4 ± 1.0	− 1.13
2385.58 ± 0.24	0.25 ± 0.04	2.80 ± 0.42	2.29 ± 0.37	2386.8 ± 1.0[f]	7.4 ± 2.0	− 2.25
2406.04 ± 0.29[a]	0.28 ± 0.04	3.09 ± 0.44	2.52 ± 0.37	2407.0 ± 1.2	6.3 ± 2.0	− 1.57
2812.07 ± 0.38[a,d]	0.09 ± 0.03	1.03 ± 0.28	0.84 ± 0.28	–	–	–
3115.34 ± 0.36[a,d]	0.19 ± 0.04	2.08 ± 0.44	1.70 ± 0.36	–	–	–
3290.76 ± 0.60[a]	0.15 ± 0.04	1.66 ± 0.40	1.35 ± 0.36	–	–	–
3789.49 ± 0.68[a]	0.16 ± 0.04	1.82 ± 0.47	1.49 ± 0.37	–	–	–

E_γ is the gamma-ray energy, $P_{E\gamma}(90°)/(\varepsilon_{E\gamma} \cdot f_{E\gamma})$ the net counts in the gamma-ray peak divided by the full-energy-peak efficiency and the gamma-ray self-absorption factor, I_R the relative intensity of the gamma-ray and $<\sigma_{E\gamma}(90°)>$ the fission-neutron spectrum-averaged partial cross section for gamma-ray production at an angle of 90° between neutron beam and detector determined with Eq. (1). *R* is the residual calculated by means of Eq. (5). Gamma lines written in bold are not yet listed in [23, 29]. The uncertainty for $P_{E\gamma}(90°)/(\varepsilon_{E\gamma} \cdot f_{E\gamma})$ is calculated from the uncertainty of the net counts of the lines $P_{E\gamma}(90°)$ and the uncertainty of the full-energy peak efficiency $\varepsilon_{E\gamma}$ (3%) The uncertainty for $<\sigma_{E\gamma}(90°)>$ is calculated from the uncertainty of $P_{E\gamma}(90°)/(\varepsilon_{E\gamma} \cdot f_{E\gamma})$ and the uncertainty of the fast neutron flux (3.5%)

[a]Gamma-ray not listed in [29] yet; any other origins than $^{139}La(n,n'\gamma)^{139}La$ excluded

[b]Maybe unresolved (n,γ) capture line of ^{139}La by Demidov at 163 keV[2]

[c]Corrected for background interference

[d](n,γ) interference above 1% corrected; contributions to net counts see text

[e]Imprecise fit at tip of ^{70}Ge triangle at 1040 keV

[d]Corrected for contribution of the $^{35}Cl(n,n'\gamma)^{35}Cl$ reaction with the partial cross section deduced from the PVC measurement, i.e. (58 ± 5) mb[18]

[e]1254 and 1257 keV (unresolved doublet by Demidov)

[f]Possible uncorrected interference by the 2390-keV line of ^{116m}In

$a_2 = 0.0020 \pm 0.0002$, $a_3 = 2.3469 \pm 0.1356$ and $a_4 = 0.0191 \pm 0.0007$ for the $PrCl_3 \cdot 7H_2O$ sample.

Due to several interferences arising from (n,γ) neutron capture reactions, the neutron self-shielding factors were determined for both samples for thermal, epithermal and fast neutrons from numerical simulations using the Monte Carlo N-Particle (MCNP, version 6.1) code [34, 35] as described in our previous work [19]. For the $LaCl_3 \cdot 7H_2O$ sample values of $f_n = 0.981$ for thermal, $f_n = 1.070$ for epithermal and $f_n = 1.014$ for fast neutrons, respectively, were obtained. For the $PrCl_3 \cdot 7H_2O$ samples values of 0.976, 1.069 and 1.014 were found for thermal, epithermal and fast neutrons, respectively. As both samples contain approximately 30 wt% of water, moderation factors f_{mod} were derived also with the MCNP code for all three considered neutron-energy ranges. In the case of the $LaCl_3 \cdot 7H_2O$ sample a value of $f_{mod} = 6.2 \pm 2.8$ for thermal and a value of $f_{mod} = 1.6 \pm 0.3$ for epithermal neutrons was found. For the $PrCl_3 \cdot 7H_2O$ sample values of 6.1 ± 2.8 and 1.6 ± 0.3 were estimated for thermal and epithermal neutrons, respectively. For the fast neutrons $f_{mod} = 1$, for both samples For the correction of (n,γ) interferences, neutron spectrum-averaged (effective) cross sections were determined by processing nuclear data of the ENDF/B-VIII.0 library [36] with the NJOY Nuclear Data Processing System (Version 2016) [37, 38]. The contributions to the net counts were calculated as described in our previous work where we report on the measurement of a $TbCl_3 \cdot 6H_2O$ sample [19].

Gamma rays of lanthanum

Fifty-four prompt gamma lines issued from the $^{139}La(n,n'\gamma)^{139}La$ reaction were measured. The gamma rays are marked accordingly in Figs. 1 and 2 and their corresponding data is provided in Table 1. Interferences with lines of the $^{35}Cl(n,\gamma)^{36}Cl$, $^{138}La(n,\gamma)^{139}La$ and $^{139}La(n,\gamma)^{140}La$ reactions are corrected with the intensities taken from [2] and the procedure described in [19]. For 8 lines relevant contributions to the net counts were corrected: 330.1 (1.3%), 495.2 (9.2%), 1370.5 (1.4%), 1595.2 (2.8%), 1600.3 (18.2%), 1625.6 (11.5%), 2812.1 (24.8%) and 3115.3 keV (23.7%). Several chlorine lines are Doppler broadened [39, 40]. The composition of the $LaCl_3 \cdot 7H_2O$ sample was verified using the data of the PVC foil measured in our work related to $CeCl_3$ [18]. The chlorine lines at 1185, 2646, 2694, 3002, 3085 and 3103 keV (see Figs. 1 and 2) free from interferences according to data in [23] were used to calculate an

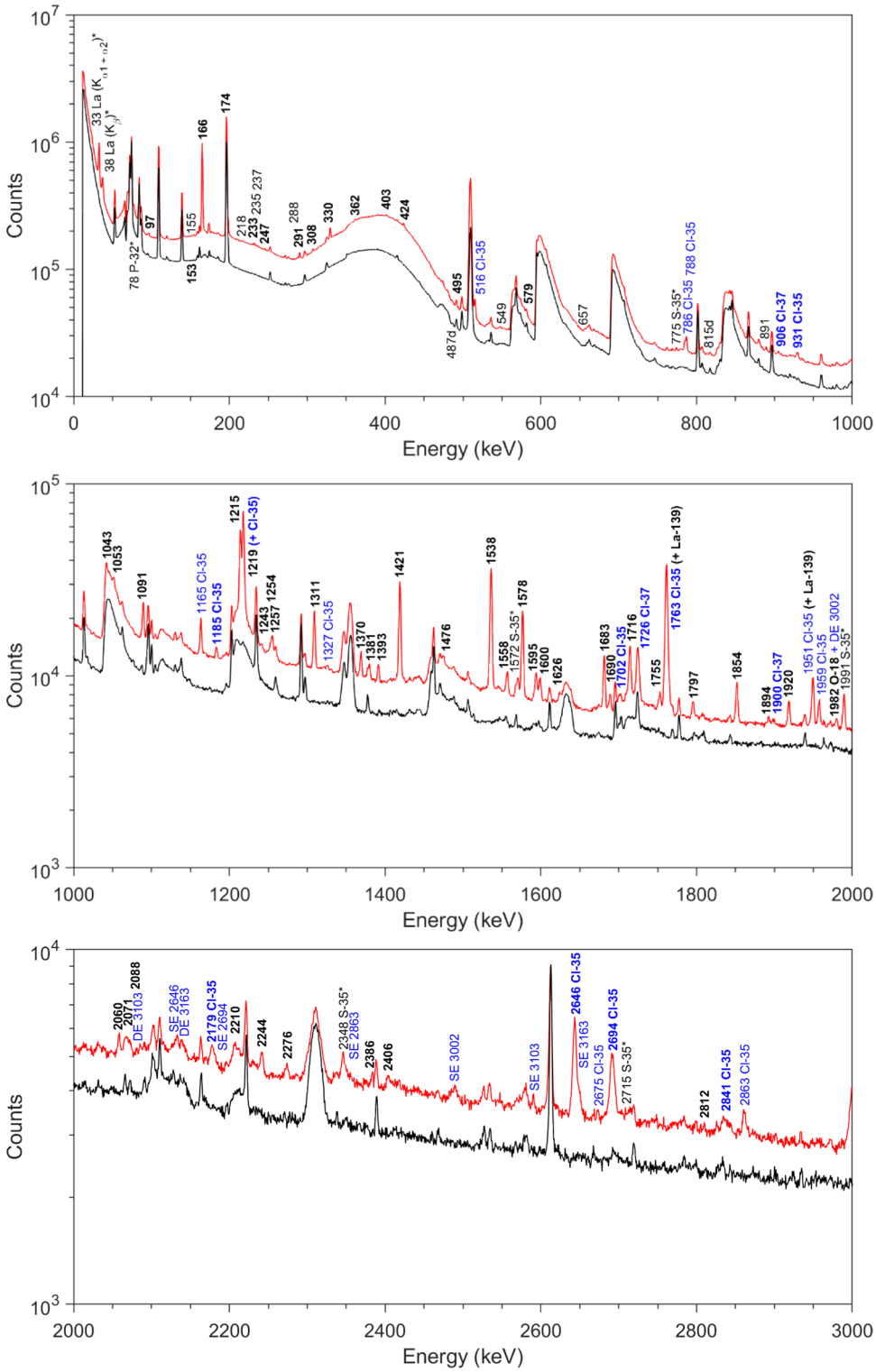

Fig. 1 Gamma-ray spectra in the energy range 0–3000 keV acquired during 39,357 s counting live time for the $LaCl_3{\cdot}7H_2O$ sample (red) and during 51,506 s for the beam background (black). Prompt gamma rays induced by (n,pγ) reactions (S-35), and (n,αγ) reactions (P-32) on Cl-35 as well as X-rays from lanthanum are written in black with an asterisk. Prompt gamma rays issued from (n,n'γ) inelastic scattering of fast neutrons on lanthanum (La-139) are written in black and bold. Prompt gamma rays from (n,γ) reactions in lanthanum (La-139) are written in black. Gamma rays of chlorine from inelastic scattering are written in bold blue. Lines in light blue are radiative capture gamma rays from Cl-35. Abbreviations SE and DE indicate single and double escape peaks, respectively. The origin of prominent lines attributed to the beam background is discussed within our former publications [12, 14]

average chlorine mass of (0.43 ± 0.02) g, which matches well with the value derived from the the stoichiometry of the sample, 0.43 g.

The intensities of the lines were determined relative to the 1420-keV line of ^{139}La and are presented together with the values given in [5] in columns 3 and 6 of Table 1. We have detected 43 of 51 lines listed in the Demidov Atlas. A total of 24 lines listed in [5] were unassigned. Of these, we observed the lines at 174.6, 232.5, 291.3, 308.3, 330.7, 363.1, 403.8, 525.2, 581.3, 1853.6, 2276.2 and 2385.6 keV. Aforementioned lines were found to belong to the ^{139}La(n,n'γ)^{139}La reaction with respect to [23, 29]. Unassigned lines at 1626.7,

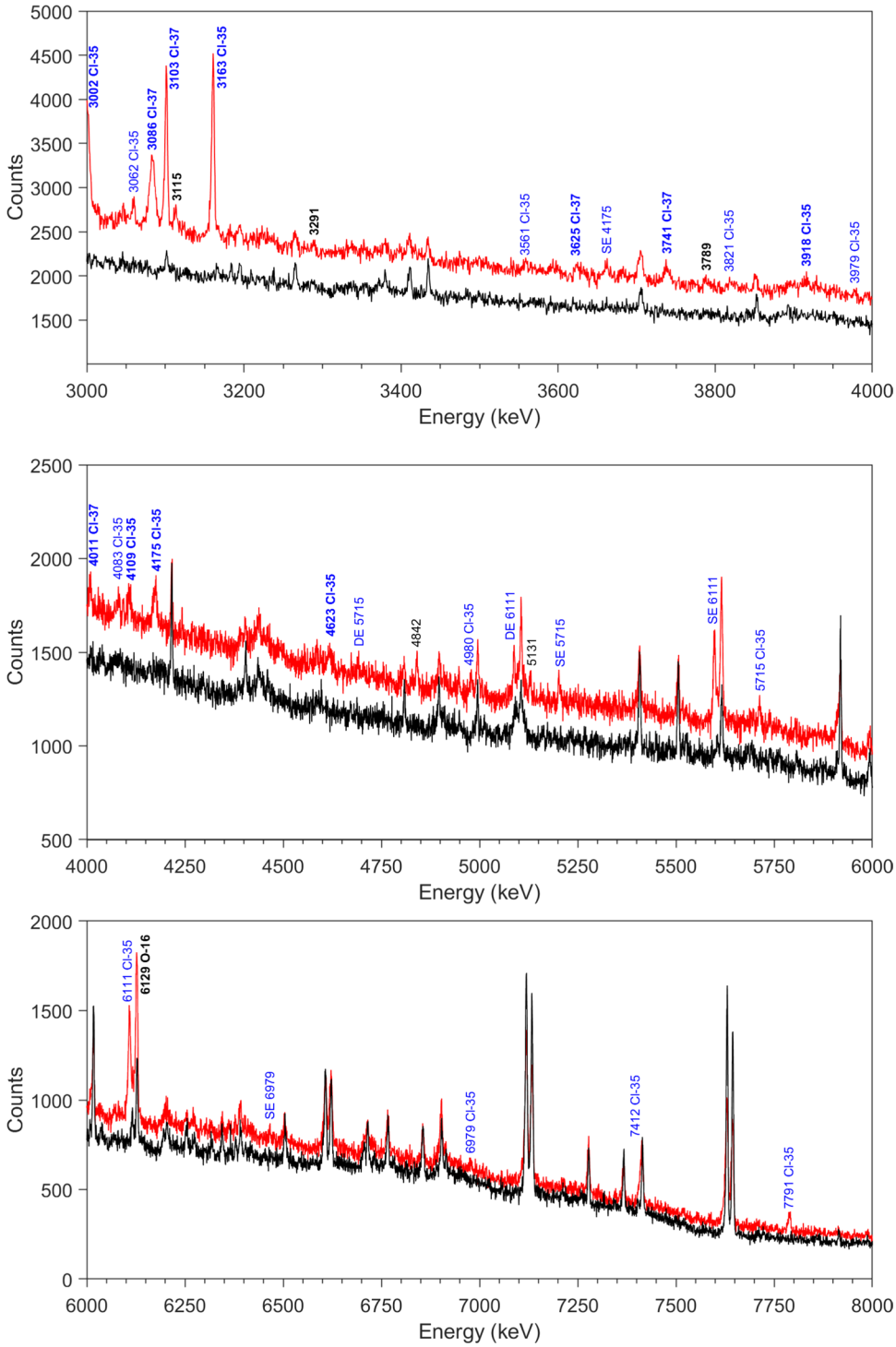

Fig. 2 Gamma-ray spectra in the energy range 3000–8000 keV acquired during 39,357 s counting live time for the $LaCl_3{\cdot}7H_2O$ sample (red) and during 51,506 s for the beam background (black). Prompt gamma rays issued from (n,n'γ) inelastic scattering of fast neutrons on lanthanum (La-139) are written in black and bold. Prompt gamma rays from (n,γ) reactions in lanthanum (La-139) are written in black. Gamma rays of chlorine from inelastic scattering are written in bold blue. Lines in light blue are radiative capture gamma rays from Cl-35. Abbreviations SE and DE indicate single and double escape peaks, respectively. The origin of prominent lines attributed to the beam background is discussed within our former publications [12, 14]

2071.4, 2210.5, 2244.6 and 2407.0 keV were observed in our measurement with missing data in [23, 29]. However, we assigned those lines also the (n,n'γ) reaction in ^{139}La since other reactions channels were carefully excluded. In fact, some of those lines could belong to a direct transition to ground state (g.s.) as corresponding levels are listed in [29] but without any gamma-ray data yet.

The lines listed at energies of 846.8, 1462.6, 1613.6, 1766.0, 1951.4, 2298.0, 2314.2 and 2356.1 keV given in [5] have not been detected in our work. For the lines at 846.8, 1462.6, 1613.6 and 2314.2 keV no assignment was done by Demidov et al. and they could be present but obscured in our measurement due to background interferences with lines of ^{56}Fe and ^{56}Mn, ^{72}Ge, ^{56}Fe and ^{14}N [12, 14]. Absence of

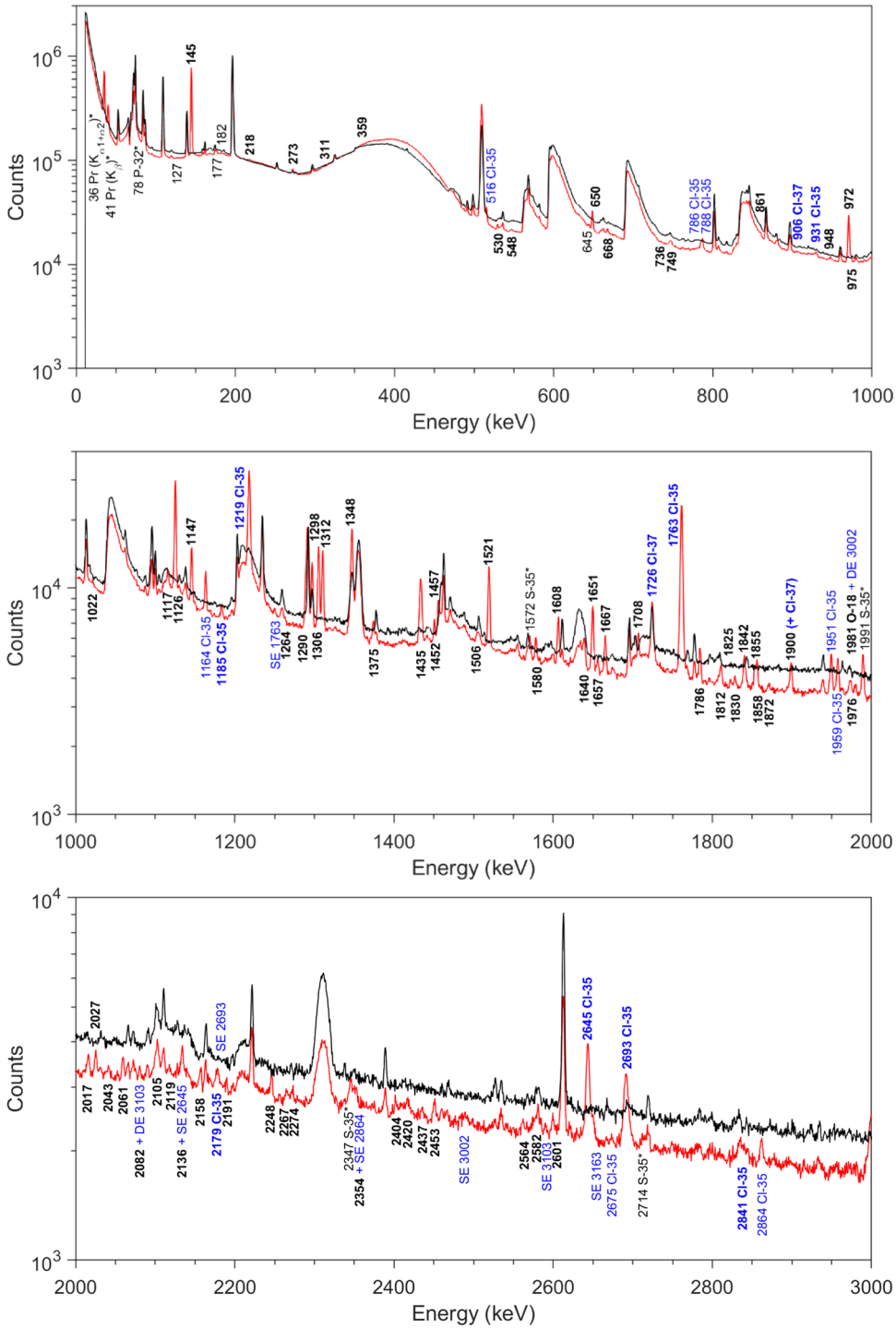

Fig. 3 Gamma-ray spectra in the energy range 0–3000 keV acquired during 22,580 s counting live time for the $PrCl_3{\cdot}7H_2O$ sample (red) and during 51,506 s for the beam background (black). Prompt gamma rays induced by (n,pγ) reactions (S-35), and (n,αγ) reactions (P-32) on Cl-35 as well as X-rays from praseodymium are written in black with an asterisk. Prompt gamma rays issued from (n,n'γ) inelastic scattering of fast neutrons on praseodymium (Pr-141) are written in black and bold. Prompt gamma rays from (n,γ) reactions in praseodymium (Pr-141) are written in black. Gamma rays of chlorine from inelastic scattering are written in bold blue. Lines in light blue are radiative capture gamma rays from Cl-35. Abbreviations SE and DE indicate single and double escape peaks, respectively. The origin of prominent lines attributed to the beam background is discussed within our former publications [12, 14]

plausible data for those lines in [23, 29] provides support that they do probably not belong to ^{139}La. The lines at 1766.0 and 1951.4 keV were not observed due to interferences from chlorine, i.e. the ^{35}Cl(n,n'γ)^{35}Cl and the ^{35}Cl(n,γ)^{36}Cl reactions. The line at 1766.0 keV belongs to a level at 1766.4 keV above g.s. and another line at 1600.3 keV was observed in this work [29]. The 1951.4-keV line as well as the line at 2456.1 keV could correspond to a direct transition to g.s. not yet listed in [23, 29]. No data is available for the 2298.0-keV line in [23, 29], but absence of this line in our work might be related to the detection limit (lanthanum mass of 0.57 g in this work vs. 18 g in [5]).

In comparison to [5] eleven new lines were identified. Only the lines at 97.1, 495.2 and 1254.1 keV are specified in [23, 29]. The 97.1-keV could not be seen by Demidov et al. as the gamma-ray threshold was set to 120 keV [5]. It

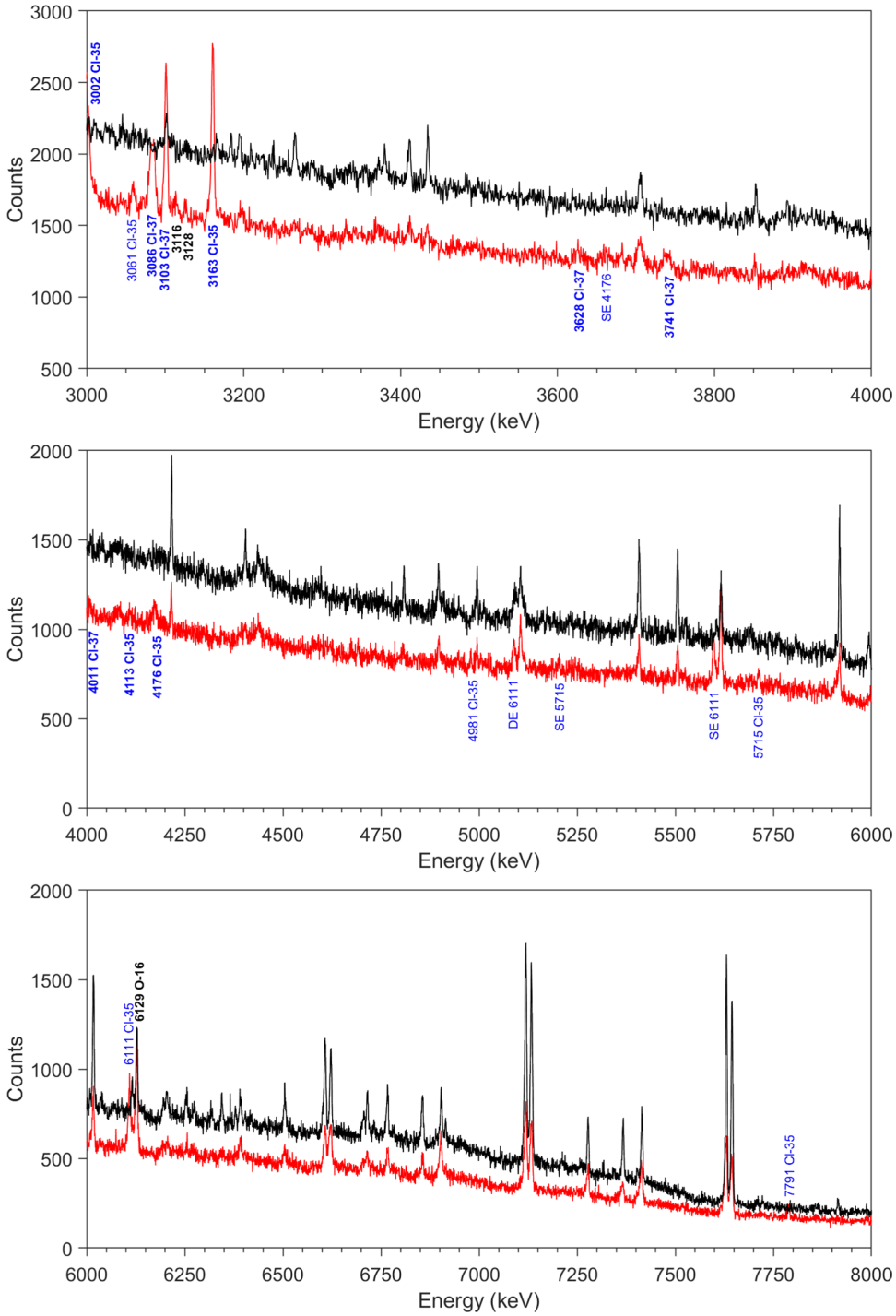

Fig. 4 Gamma-ray spectra in the energy range 3000–8000 keV acquired during 22,580 s counting live time for the $PrCl_3{\cdot}7H_2O$ sample (red) and during 51,506 s for the beam background (black). Prompt gamma rays issued from (n,n'γ) inelastic scattering of fast neutrons on praseodymium (Pr-141) are written in black and bold. Gamma rays of chlorine from inelastic scattering are written in bold blue. Lines in light blue are radiative capture gamma rays from Cl-35. Abbreviations SE and DE indicate single and double escape peaks, respectively. The origin of prominent lines attributed to the beam background is discussed within our former publications [12, 14]

is unclear why the 495.2-keV line had not been observed in Demidov´s measurement, since another line at 232.6 keV from the same level (2032.8 keV above g.s. [29]) was observed also by Demidov et al. The line at 1254.1 keV represents a resolved doublet in our work with the line at 1256.6 keV and it could not be observed by Demidov et al. due to the worse detector resolution. For the new lines identified at 153.4, 246.5, 1242.8, 2087.6, 2812.1, 3115.3, 3290.8 and 3789.5 keV no data is available in [23, 29]. However, due to acceptable peak statistics ranging between 9.5 and 26.7% and the careful exclusion of any other reaction channels, these lines are proposed as new (n,n´γ) lines of ^{139}La. In particular, the lines at 2812.1, 3115.3 and 3789.5 keV could indeed belong to direct transitions to g.s., since the required level energies are known from ^{139}La(γ,γ´)^{139}La reactions [29, 41] with incident gamma-ray energies between

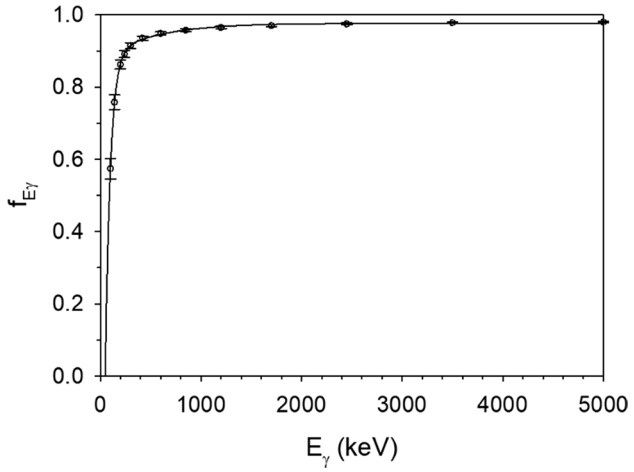

Fig. 5 Dependence of the gamma-ray self-absorption factor $f_{E\gamma}$ on the gamma-ray energy E_γ for the $LaCl_3{\cdot}7H_2O$ sample. The data points were obtained from NIST XCOM [32, 33].The solid line displays the fit of the data after Eq. (3)

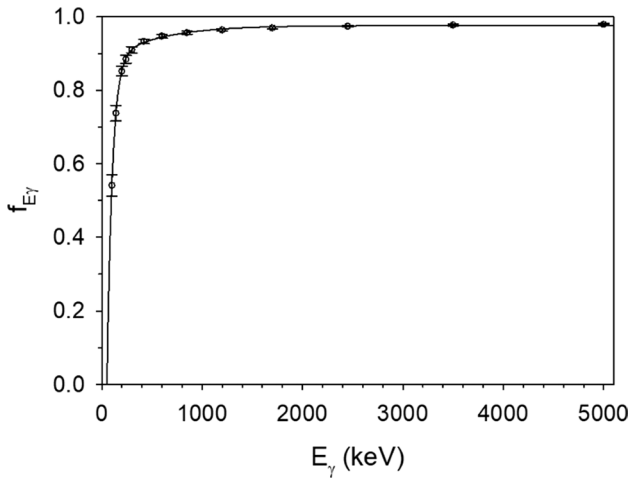

Fig. 6 Dependence of the gamma-ray self-absorption factor $f_{E\gamma}$ on the gamma-ray energy E_γ for the $PrCl_3{\cdot}7H_2O$ sample. The data points were obtained from NIST XCOM [32, 33]. and the fit of the data after Eq. (3) is shown by The solid line displays the it of the data after Eq. (3)

1.2 and 4.1 MeV, overlapping well with the mean neutron energy at FaNGaS.

The relative intensities derived in our work are plotted versus the values listed in [5] in Fig. 7. The relation between the two sets of data is expressed by

$$I_R = a \cdot \left(I_{RD}\right)^b \tag{4}$$

with $a = 0.86 \pm 0.12$ and $b = 1.02 \pm 0.05$.

The average value of the intensity ratio, i.e. I_R/I_{RD}, is 0.95 ± 0.27 and shows a good agreement between the two

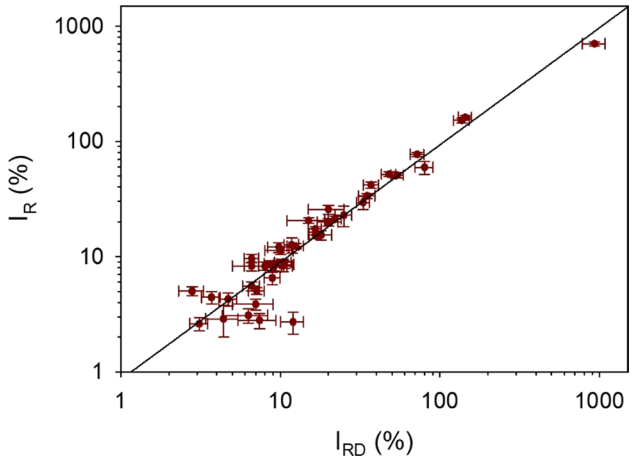

Fig. 7 Correlation between the relative intensities I_R of the prompt gamma rays produced by inelastic scattering (n,n'γ) reactions of fast neutrons on lanthanum (La-139) determined in this work and the relative intensities I_{RD} given in the Demidov Atlas [5]. The solid line represents the fit of the data with Eq. (4)

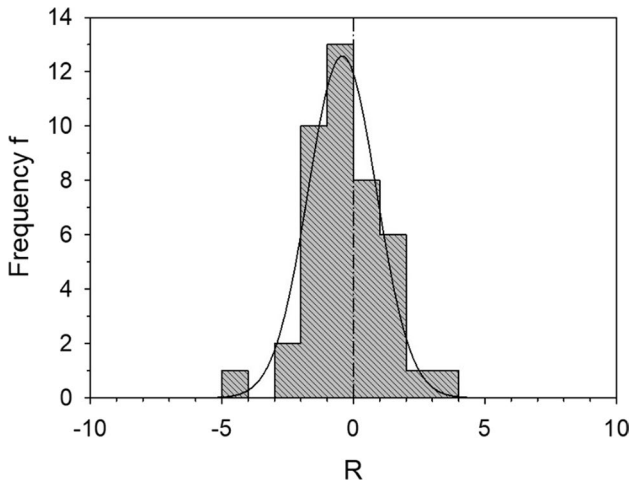

Fig. 8 Histogram of the residuals R, calculated with Eq. (5) in units of standard deviation [σ], showing the agreement between the relative intensities of gamma rays from the $^{139}La(n,n'\gamma)^{139}La$ reaction derived in this work with the data listed in [5]. The solid line displays the fit of the data with a Gaussian

measurements. To check the consistency further, the two data sets are shown in Fig. 8 as a histogram of the residuals R in units of standard deviation [σ], calculated as:

$$R = \frac{I_R - I_{RD}}{\sqrt{\left(s_{I_R}\right)^2 + \left(s_{I_{RD}}\right)^2}} \tag{5}$$

The fit with a Gaussian indicates an agreement between the data at the 1.3σ level. The shift of the centroid by −0.42 show a relevant systematic effect.

The partial cross sections for gamma-ray production, calculated by means of Eq. (1) with a flux of $(1.13 \pm 0.04) \times 10^8$ cm^{-2} s^{-1}, are given in column 4 of Table 1.

Gamma rays of praseodymium

Seventy one lines assigned to the ^{141}Pr(n,n'γ)^{141}Pr reaction were measured. They are labeled in Figs. 3 and 4 and their corresponding data is provided in Table 2. Interferences of radiative capture lines from the ^{35}Cl(n,γ)^{36}Cl and ^{141}Pr(n,γ)^{142}Pr reactions are corrected using the intensities given in[2] and the procedure described in [19]. For 9 lines relevant contributions to the net counts were corrected: 359.3 (3.7%), 547.9 (33.9%), 974.6 (8.1%), 1375.2 (1.4%), 1640.2 (2.2%), 1785.9 (1.5%), 2042.9 (6.4%), 2158.3 (6.6%), 3115.6 keV (18.6%). The composition of the $PrCl_3 \cdot 7H_2O$ sample was checked in the same way as for the $LaCl_3 \cdot 7H_2O$ sample (see above). The average chlorine mass was determined to (0.43 ± 0.01) g and found to agree well with the value derived from the sample stochiometry, 0.42 g.

Relative intensities were determined using the 1126-keV line of ^{141}Pr as reference line (100%). They are presented together with the values given in [5] in columns 3 and 6 of Table 2. We have detected 57 of 77 lines listed in [5]. A total of 23 lines listed in [5] had been listed without any assignment. Of these, we observed the lines at 218.3, 273.3, 749.2, 861.5, 1023.1, 2027.1, 2061.4, 2136.2, 2159.7, 2352.8, 2403.9, 2453.6, 2581.2 and 2603.1 keV. Aforementioned lines were found to belong to the ^{141}Pr(n,n'γ)^{141}Pr reaction with respect to [23, 30]. Another line at 1825.2 keV [5], unspecified in [23, 30], was also related to inelastic scattering on ^{141}Pr in our work as all other origins were carefully ruled out.

For the lines observed at 1506.0, 2082.1, 2104.8, 2135.5 and 2354.3 keV escape-peak interferences were identified. These peaks were interfered by the lines at 2017.2 (^{141}Pr, SE), 3103.1 (^{37}Cl, DE), 2614 (^{208}Pb, SE), 2645.3 (^{35}Cl, SE) and 2864 keV (^{35}Cl, SE). The contributions to the net counts of the aforementioned lines were estimated using the correction curves given in [18]: $(3.5 \pm 0.5\%)$ for the 1506.0-, $(56 \pm 18\%)$ for the 2082.1-, $(60 \pm 4\%)$ for the 2104.8-, $(41 \pm 3\%)$ for the 2135.5- and $(17.6 \pm 3.6\%)$ for the 2354.3-keV line.

The 20 lines listed at energies of 179.6, 268.3, 277.5, 302.1, 339.9, 352.7, 523.6, 558.6, 723.6, 893.0, 981.7, 1140.3, 1292.6, 1696.8, 1961.9, 2282.9, 2313.8, 2414.4, 2462.4, and 2559.6 keV given in [5] have not been observed in our measurement. For all of the aforementioned lines plausible data is provided in [23, 30], except the lines at 179.6, 268.3, 277.5, 2282.9, 2414.4, 2462.4 and 2559.6 keV. At these energies no gamma-ray peak with relevant statistics was observed in our spectrum. Missing data in [23, 30] could provide support that these lines probably do not belong to ^{141}Pr. The unobserved lines listed at energies of 302.1, 339.9, 352.7, 523.6, 558.6, 723.6 and 893.0 keV in [5], had relative intensities ranging between 1.3 and 4.0%. In fact, the level of many of those lines was also excited in our measurements. Absence of these lines, however, is attributed to the lower praseodymium mass irradiated (0.56 g in our work vs. 9.2 g in [5]). The lines at 981.7, 1140.3, 1292.6, 1696.8, 1961.9 and 2313.8 keV could not be uniquely identified in this work due to background interferences with ^{208}Pb, ^{70}Ge, ^{40}Ar, ^{116m}In, ^{74}Ge, ^{35}Cl and ^{14}N. The line at 1140.3 keV is not specified in [23, 30]. For this aforementioned line as well as the lines at 2414.4 and 2559.6 keV, respectively, definitely a mistake by Demidov et al. must be concluded, since neither the level energies nor the gamma-ray energies provided in [5] are found in [23, 30].

On the other hand, compared to [5] we have identified 14 new gamma lines. These include the lines at 311.2, 948.5, 974.6, 1264.3, 1872.3, 2042.9, 2082.1, 2119.1, 2267.1, 2419.5, 2437.1, 2563.6, 3111.6 and 3127.7 keV. All of the aforementioned lines are specified in [23, 30]. The lines at 2414.4 and 2559.6 keV in [5] could correspond to the lines observed at 2419.5 and 2563.6 keV in our work. The 974.6-keV line could not be uniquely seen by Demidov et al. due to a doublet structure in [5] with the line listed at 972.2 keV. The 1264.3-keV line was emitted from a level at 2382.2 keV above g.s. [30], from which we also observed the line at 861.0 keV. As the latter one, however, was observed by Demidov et al. it is surprising and unclear why the line at 1264.3 keV had not been observed. The same observation could also apply to the lines at 311.2, 1872.3, 2042.9 and 2437.2 keV, for which other lines from the respective excited levels had been observed by Demidov et al. We attribute the absence of the remaining lines to deviations in the different level excitation due to the different neutron-energy spectra.

The intensity plot is shown in Fig. 9. The values have been fitted with Eq. (4), yielding the coefficients $a = 0.86 \pm 0.07$ and $b = 1.00 \pm 0.03$.

The average value of the intensity ratio, i.e. I_R/I_{RD}, is 0.91 ± 0.27 indicating a good agreement between the two sets of data. The residual histogram is depicted in Fig. 10. The Gaussian fit of the data results in an agreement level of 1.3σ.The Gaussian centroid is shifted by −0.46, pointing out a systematic effect.

The partial cross sections for the production of identified gamma-rays, averaged over the fast-neutron spectrum and calculated by means of Eq. (1) with a flux of $(1.13 \pm 0.04) \times 10^8$ cm^{-2} s^{-1}, are given in column 4 of Table 2.

Table 2 Prompt gamma rays of ^{141}Pr induced by inelastic scattering of fast neutrons

This work				From demidov atlas [5]		R
E_γ (keV)	$P_{E\gamma}$ (90°)/$(\varepsilon_{E\gamma}.f_{E\gamma})\times10^{-8}$ (count)	I_R(relative) (%)	$<\sigma_{E\gamma}$ (90°)> (mb)	E_γ (keV)	I_R (relative) (%)	
145.30 ± 0.03	54 ± 2	812 ± 40	889 ± 45	145.45 ± 0.05	1200 ± 200	− 1.90
218.42 ± 0.11	0.19 ± 0.05	2.80 ± 0.81	3.06 ± 0.81	218.3 ± 0.5	3.2 ± 0.9	− 0.33
272.88 ± 0.04[a]	0.79 ± 0.05	11.8 ± 0.8	12.9 ± 0.9	273.3 ± 0.2	18 ± 4	− 1.52
311.22 ± 0.36	0.16 ± 0.03	2.34 ± 0.42	2.56 ± 0.49	–	–	–
359.35 ± 0.11[b]	0.38 ± 0.05	5.68 ± 0.75	6.22 ± 0.85	359.8 ± 0.6	4.1 ± 0.8	1.45
530.11 ± 0.11[a]	0.15 ± 0.03	2.21 ± 0.48	2.42 ± 0.49	530.88 ± 0.10	2.4 ± 0.7	− 0.23
547.86 ± 0.23[b]	0.12 ± 0.02	1.85 ± 0.33	2.02 ± 0.34	546.4 ± 0.3	2.0 ± 0.4	− 0.30
649.52 ± 0.04	2.44 ± 0.10	36 ± 2	40 ± 2	650.34 ± 0.10	35 ± 8	0.17
668.48 ± 0.07[a]	0.26 ± 0.03	3.90 ± 0.51	4.27 ± 0.51	668.88 ± 0.10	6.0 ± 1.0	− 1.87
735.73 ± 0.29	0.12 ± 0.03	1.73 ± 0.52	1.90 ± 0.48	736.0 ± 0.3	2.8 ± 0.4	− 1.63
748.72 ± 0.15[a]	0.18 ± 0.03	2.62 ± 0.39	2.87 ± 0.49	749.21 ± 0.10	5.8 ± 0.6	− 4.42
860.96 ± 0.12[a]	0.10 ± 0.02	1.52 ± 0.37	1.66 ± 0.33	861.5 ± 0.2	2.1 ± 0.4	− 1.07
948.47 ± 0.13	0.23 ± 0.04	3.49 ± 0.60	3.82 ± 0.68	–	–	–
971.64 ± 0.05[a]	5.63 ± 0.18	84 ± 4	92 ± 4	972.24 ± 0.10	83 ± 8[c]	− 3.14
974.64 ± 0.11[b]	0.37 ± 0.03	5.51 ± 0.49	6.04 ± 0.53	–	–	–
1022.47 ± 0.14	0.09 ± 0.02	1.29 ± 0.31	1.42 ± 0.32	1023.1 ± 0.2	3.7 ± 0.6	− 3.56
1117.10 ± 0.10[a]	0.50 ± 0.05	7.50 ± 0.74	8.22 ± 0.87	1117.65 ± 0.10	7.6 ± 0.7	− 0.09
1126.40 ± 0.05	6.70 ± 0.21	100	110 ± 5	1126.90 ± 0.10	100	–
1146.80 ± 0.06	2.30 ± 0.09	34 ± 2	38 ± 2	1147.24 ± 0.10	34 ± 4	0.07
1264.30 ± 0.24	0.11 ± 0.02	1.68 ± 0.33	1.84 ± 0.34	–	–	–
1290.31 ± 0.08	1.39 ± 0.08	21 ± 1	23 ± 1	1290.0 ± 0.4	27 ± 10	− 0.62
1298.18 ± 0.06[a]	2.02 ± 0.09	30 ± 2	33 ± 2	1298.74 ± 0.10	33 ± 4	− 0.64
1306.45 ± 0.06	3.42 ± 0.11	51 ± 3	56 ± 3	1306.85 ± 0.10	50 ± 5	0.20
1311.61 ± 0.06	3.31 ± 0.11	49 ± 3	54 ± 3	1312.13 ± 0.10	51 ± 5	− 0.29
1347.98 ± 0.06[a]	3.62 ± 0.21	54 ± 4	59 ± 4	1348.70 ± 0.10	47 ± 4	1.29
1375.23 ± 0.11[b]	0.54 ± 0.05	8.00 ± 0.75	8.76 ± 0.87	1375.7 ± 0.3	12 ± 3	− 1.29
1434.83 ± 0.09[a]	3.00 ± 0.13	45 ± 3	49 ± 3	1435.34	50 ± 5	− 0.91
1451.73 ± 0.09	0.61 ± 0.05	9.09 ± 0.71	9.95 ± 0.89	1452.21 ± 0.10	13 ± 2	− 1.84
1456.89 ± 0.08[a]	1.11 ± 0.06	16.6 ± 1.1	18.2 ± 1.2	1457.52 ± 0.10	17 ± 2	− 0.18
1506.04 ± 0.19	0.30 ± 0.03	4.47 ± 0.50	4.89 ± 0.52	1506.9 ± 0.5	6.1 ± 0.2	− 3.04
1520.68 ± 0.07	3.29 ± 0.11	49 ± 3	54 ± 3	1521.13 ± 0.10	51 ± 5	− 0.34
1579.61 ± 0.09	0.63 ± 0.04	9.45 ± 0.68	10.3 ± 0.7	1580.2 ± 1.0	6.3 ± 0.7	3.23
1607.78 ± 0.08	1.37 ± 0.05	20 ± 1	22 ± 1	1608.30 ± 0.10	20 ± 2	0.21
1640.18 ± 0.11[a,b]	0.50 ± 0.05	7.48 ± 0.74	8.19 ± 0.87	1641.2 ± 0.2	7.2 ± 0.8	0.26
1651.03 ± 0.08	2.05 ± 0.08	31 ± 2	33 ± 2	1651.48 ± 0.10	33 ± 3	− 0.71
1657.19 ± 0.14	0.31 ± 0.03	4.66 ± 0.51	5.10 ± 0.52	1658.0 ± 0.2	3.2 ± 0.9	1.91
1666.81 ± 0.08	1.02 ± 0.05	15.2 ± 0.9	16.7 ± 1.0	1667.28 ± 0.10	13 ± 3	0.71
1708.19 ± 0.09	0.76 ± 0.04	11.3 ± 0.7	12.4 ± 0.8	1708.75 ± 0.10	14 ± 3	− 0.87
1785.90 ± 0.09[b]	0.85 ± 0.05	12.8 ± 0.9	14 ± 1	1786.45 ± 0.10	16 ± 2	− 1.48
1811.92 ± 0.14[a]	0.28 ± 0.03	4.11 ± 0.43	4.50 ± 0.51	1812.9 ± 0.2	5.8 ± 0.6	− 2.28
1824.57 ± 0.27[c]	0.14 ± 0.03	2.09 ± 0.45	2.29 ± 0.50	1825.2 ± 0.3	2.0 ± 0.5	0.13
1829.99 ± 0.22	0.28 ± 0.04	4.11 ± 0.63	4.50 ± 0.66	1830.5 ± 0.3	3.4 ± 0.4	0.95
1841.80 ± 0.11	0.89 ± 0.05	13.2 ± 0.9	14.5 ± 0.9	1842.22 ± 0.10	12 ± 2	0.56
1854.68 ± 0.16	0.45 ± 0.07	6.74 ± 1.04	7.38 ± 1.18	1854.9 ± 0.6	7 ± 2	− 0.12
1857.62 ± 0.14	0.65 ± 0.07	9.72 ± 1.10	10.7 ± 1.2	1858.4 ± 0.5	9 ± 2	0.32
1872.30 ± 0.24	0.17 ± 0.03	2.59 ± 0.48	2.83 ± 0.51	–	–	–
1900.19 ± 0.11[f]	0.58 ± 0.04	8.62 ± 0.65	9.44 ± 0.73	1900.90 ± 0.10	11 ± 2	− 1.13

Table 2 (continued)

This work				From demidov atlas [5]		R
E_γ (keV)	$P_{E\gamma}$ (90°)/$(\varepsilon_{E\gamma}{\cdot}f_{E\gamma})\times10^{-8}$ (count)	I_R(relative) (%)	$<\sigma_{E\gamma}$ (90°)> (mb)	E_γ (keV)	I_R (relative) (%)	
1975.79 ± 0.29	0.26 ± 0.05	3.87 ± 0.70	4.23 ± 0.83	1975.7 ± 0.3	5.2 ± 0.6	− 1.45
2017.21 ± 0.19[a]	0.19 ± 0.03	2.81 ± 0.40	3.07 ± 0.50	2018.8 ± 0.5	4.4 ± 0.6	− 2.20
2026.63 ± 0.15	0.30 ± 0.03	4.55 ± 0.51	4.98 ± 0.53	2027.1 ± 0.3	11 ± 3	− 2.12
2042.87 ± 0.31[b]	0.13 ± 0.02	1.89 ± 0.33	2.07 ± 0.33	–	–	–
2060.97 ± 0.16	0.33 ± 0.03	4.90 ± 0.48	5.37 ± 0.52	2061.4 ± 0.3	3.7 ± 0.6	1.57
2082.08 ± 0.29[d]	0.05 ± 0.01	0.80 ± 0.20	0.88 ± 0.18	–	–	–
2104.82 ± 0.19[a,d]	0.19 ± 0.01	2.84 ± 0.23	3.11 ± 0.20	2105.3 ± 1.0	2.2 ± 0.6	0.99
2119.11 ± 0.34	0.13 ± 0.03	1.87 ± 0.39	2.05 ± 0.48	–	–	–
2135.54 ± 0.15[d]	0.32 ± 0.02	4.81 ± 0.39	5.27 ± 0.38	2136.2 ± 0.7	3.0 ± 0.9	1.84
2158.33 ± 0.24[b]	0.21 ± 0.03	3.11 ± 0.41	3.40 ± 0.50	2159.7 ± 0.5	4.3 ± 0.8	− 1.33
2191.22 ± 0.27	0.11 ± 0.03	1.60 ± 0.41	1.75 ± 0.48	2192.7 ± 1.5	3.3 ± 0.7	− 2.10
2247.71 ± 0.15	0.31 ± 0.03	4.64 ± 0.48	5.08 ± 0.52	2248.8 ± 0.5	5.3 ± 0.8	− 0.70
2267.07 ± 0.43	0.12 ± 0.03	1.72 ± 0.44	1.88 ± 0.47	–	–	–
2273.95 ± 0.36[a]	0.08 ± 0.02	1.21 ± 0.30	1.32 ± 0.33	2274.6 ± 0.5	1.9 ± 0.6	− 1.04
2354.29 ± 0.36[d]	0.18 ± 0.03	2.64 ± 0.49	2.89 ± 0.49	2352.8 ± 0.5	2.0 ± 0.9	0.63
2403.74 ± 0.33	0.14 ± 0.03	2.11 ± 0.46	2.31 ± 0.50	2403.9 ± 0.5	3.0 ± 0.9	− 0.88
2419.53 ± 0.37	0.15 ± 0.04	2.29 ± 0.56	2.51 ± 0.67	–	–	–
2437.12 ± 0.32	0.15 ± 0.03	2.20 ± 0.39	2.41 ± 0.49	–	–	–
2452.70 ± 0.19	0.29 ± 0.02	4.40 ± 0.41	4.82 ± 0.37	2453.6 ± 1.0	4 ± 2	0.20
2563.55 ± 0.32	0.12 ± 0.02	1.84 ± 0.34	2.02 ± 0.34	–	–	–
2582.26 ± 0.25[a]	0.16 ± 0.02	2.32 ± 0.32	2.54 ± 0.33	2581.2 ± 1.5	3.1 ± 0.9	− 0.82
2601.50 ± 0.25	0.21 ± 0.03	3.11 ± 0.43	3.40 ± 0.50	2603.1 ± 1.0	4 ± 2	− 0.44
3115.56 ± 0.70[b]	0.09 ± 0.03	1.40 ± 0.40	1.54 ± 0.51	–	–	–
3127.71 ± 0.43	0.11 ± 0.03	1.67 ± 0.44	1.83 ± 0.50	–	–	–

E_γ is the gamma-ray energy, $P_{E\gamma}(90°)/(\varepsilon_{E\gamma}{\cdot}f_{E\gamma})$ the net counts in the gamma-ray peak divided by the full-energy-peak efficiency and the gamma-ray self-absorption factor, I_R the relative intensity of the gamma-ray and $<\sigma_{E\gamma}(90°)>$ the fission-neutron spectrum-averaged partial cross section for gamma-ray production at an angle of 90° between neutron beam and detector determined with Eq. (1). R is the residual calculated by means of Eq. (5). The gamma line written in bold is not yet listed in [23, 30]. The uncertainty for $P_{E\gamma}(90°)/(\varepsilon_{E\gamma}{\cdot}f_{E\gamma})$ is calculated from the uncertainty of the net counts of the lines $P_{E\gamma}(90°)$ and the uncertainty of the full-energy peak efficiency $\varepsilon_{E\gamma}$ (3%) The uncertainty for $<\sigma_{E\gamma}(90°)>$ is calculated from the uncertainty of $P_{E\gamma}(90°)/(\varepsilon_{E\gamma}{\cdot}f_{E\gamma})$ and the uncertainty of the fast neutron flux (3.5%)

[a]Corrected for background interference

[b](n,γ) interference above 1% corrected; contributions to net counts see text

[c]972 and 975 keV (unresolved doublet by Demidov)

[d]Corrected for escape peak interference

[e]Gamma-ray not listed in [30] yet; any other origins than $^{141}Pr(n,n'\gamma)^{141}Pr$ excluded

[f]Corrected for contribution of the $^{37}Cl(n,n'\gamma)^{37}Cl$ reaction with the partial cross section deduced from the $CeCl_3$ measurement, i.e. (2.38 ± 0.56) mb[18]

Prompt gamma rays of oxygen and chlorine

The partial cross sections of the prompt gamma lines of oxygen and chlorine were also determined by means of Eq. (1). For the 1981-keV line from $^{18}O(n,n'\gamma)^{18}O$, values of 172 ± 22 mb and 180 ± 26 mb, were derived from the $LaCl_3{\cdot}7H_2O$ and the $PrCl_3{\cdot}7H_2O$ spectrum, respectively. Values of 2.56 ± 0.29 mb and 2.69 ± 0.40 mb were derived for the 6129-keV line from the $^{16}O(n,n'\gamma)^{16}O$ reaction. Taking the uncertainties into account, aforementioned values are in good agreement with the values achieved in our work on $CaCO_3$ [17], i.e. 201 ± 28 mb and 2.20 ± 0.37 mb, respectively. Additionally, they also agree well with the values obtained in our previous work on $TbCl_3{\cdot}6H_2O$, i.e. 213 ± 40 mb and 2.22 ± 0.31 mb [19]. The 1981-keV line was corrected for the contribution of the double escape peak of the 3002-keV line (^{35}Cl) in both cases.

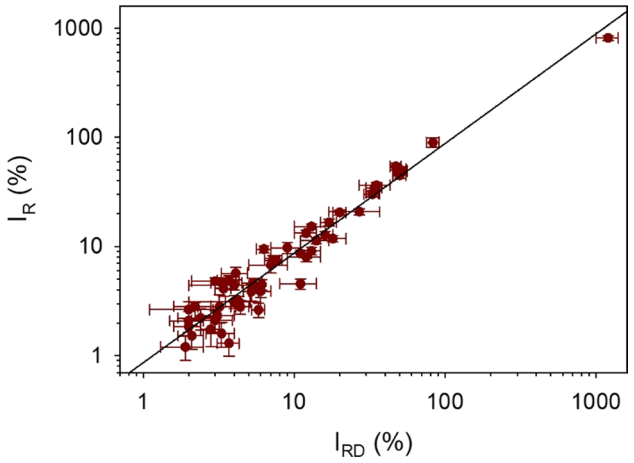

Fig. 9 Correlation between the relative intensities I_R of the prompt gamma rays generated by inelastic scattering (n,n'γ) reactions of fast neutrons on praseodymium (Pr-141) measured in this work and the relative intensities I_{RD} listed in the Demidov Atlas [5]. The solid line shows the fit of the data with Eq. (4)

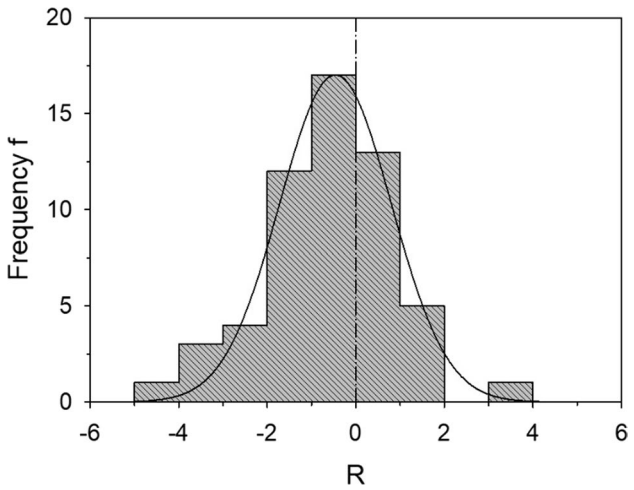

Fig. 10 Histogram of the residuals *R*, calculated with Eq. (5) in units of standard deviation [σ], showing the agreement between the relative intensities of prompt gamma rays from the ^{141}Pr(n,n'γ)^{141}Pr reaction derived in this work with the data listed in [5]. The solid line displays the fit of the data with a Gaussian

For chlorine, 29 lines were observed in the $LaCl_3{\cdot}7H_2O$ measurement, whereas the lines at 1702, 3918 and 4623 from the ^{35}Cl(n,n'γ)^{35}Cl, the line at 1900 keV from the ^{37}Cl(n,n'γ)^{37}Cl and the 775-keV line from the ^{35}Cl(n,pγ)^{35}S reactions, respectively, were not observed in the $PrCl_3{\cdot}7H_2O$ measurement, due to a lower counting time. The ratios of measured partial cross sections to the values obtained in our previous work on $CeCl_3$ [18] are shown in Fig. 11. The data of both measurements agree well with each other considering the associated uncertainties. Larger deviations for a few lines are reasoned in poor counting statistics.

Detection limit

In this work, the detection limit (DL) is defined as the smallest amount of a pure element that is irradiated over a certain time and that results in a net signal above the background with a certain standard deviation σ. The value of the DL can be determined with Eq. (1) from the minimum peak area $P_{E\gamma}(c)$ that could be expressed according to [42] as:

$$P_{E\gamma}(c) = \frac{\sqrt{2 \cdot B_{E\gamma}}}{c} \tag{6}$$

where $B_{E\gamma}$ is the area of the background below the gamma line of interest and c a predefined value for the relative uncertainty of the peak area. As a small sample mass is expected, the neutron self-shielding and gamma rays self-absorption can be neglected, i.e., $f_n = 1$ and $f_{E\gamma} = 1$ in Eq. (1).

The DL of lanthanum and praseodymium was calculated for the most intense gamma line and for a counting live time of 12 h. The HYPERMET-PC [22] software was used to estimate the value of $B_{E\gamma}$ from the beam background. For a value of $c = 0.5$ in Eq. (6) corresponding to a peak area uncertainty of 50%, the smallest amount of pure element that can be detected is 0.6 mg for lanthanum (^{139}La, $E_\gamma = 165.7$ keV, $<\sigma_{E\gamma}(90°)> = 574$ mb) and 0.4 mg for praseodymium (^{141}La, $E_\gamma = 145.3$ keV, $<\sigma_{E\gamma}(90°)> = 889$ mb).

Conclusions

Prompt gamma rays of lanthanum and praseodymium induced by inelastic scattering reactions were measured with the FaNGaS instrument by irradiating a $LaCl_3{\cdot}7H_2O$ and a $PrCl_3{\cdot}7H_2O$ sample with fission neutrons. For the correction of relevant interferences arising from (n,γ) neutron capture lines the previously redetermined thermal and epithermal neutron-flux values given in [19] were used along with the correction procedure described within [19].

We identified 54 lines from the ^{139}La(n,n'γ)^{139}La and 71 lines from the ^{141}Pr(n,n'γ)^{141}Pr reaction, respectively. Relative intensities as well as fast-neutron spectrum-averaged partial production cross sections of the aforementioned gamma rays were presented. Compared to the work of Demidov et al. [5] additional gamma lines (11 for lanthanum and 14 for praseodymium) were detected due to the better energy resolution of our detector and a higher mean excitation neutron-energy. Furthermore, as 13 lines of lanthanum and 1 line of praseodymium are unreported in [23] yet, this work can help to expand the level and decay schemes of

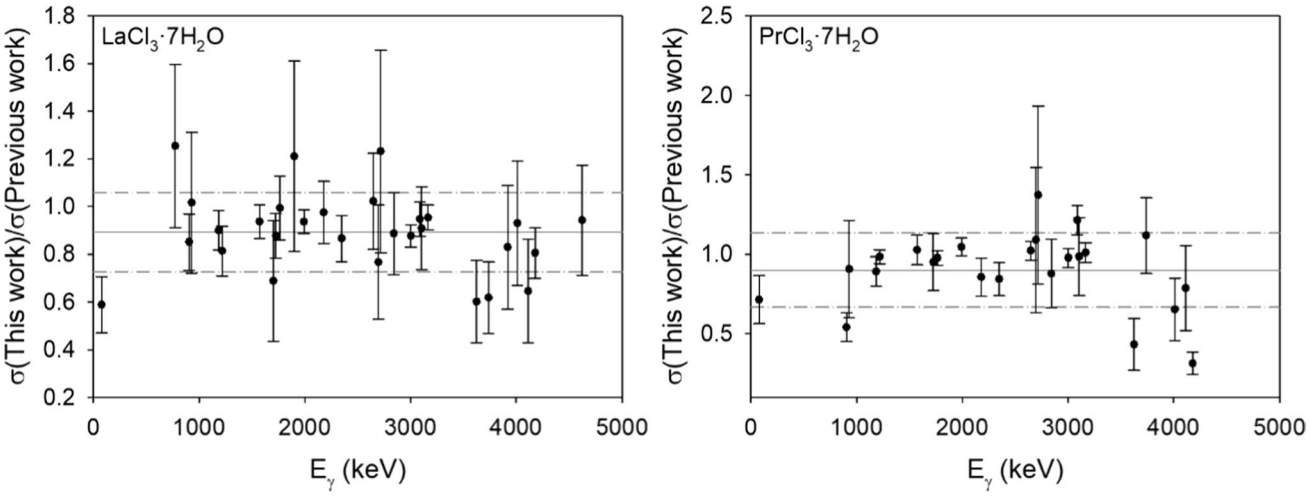

Fig. 11 Ratio of gamma-ray production cross sections $<\sigma_{E\gamma}(90°)>$ in mb for chlorine lines from (n,n'γ) and (n,pγ) reactions obtained in this work compared to these obtained in our previous work [18]. The comparison with the $LaCl_3 \cdot 7H_2O$ measurement is depicted on the left, the comparison with the $PrCl_3 \cdot 7H_2O$ measurement on the right side. The solid lines represent the mean value of the ratios, i.e. 0.89 ± 0.17 and 0.90 ± 0.23, respectively, while the dash-dotted lines display the corresponding error margins corresponding to one standard deviation

these elements. The agreement of our relative intensities (1.3σ level for both measurements) is in reasonable agreement with the values provided in [5]. The detection limits of lanthanum and praseodymium were determined as 0.6 and 0.4 mg, respectively, for a counting time of 12 h. Furthermore, the partial production cross sections for the lines of oxygen and chlorine match well with the values obtained in [17–19].

Supplementary Information The online version contains supplementary material available at https://doi.org/10.1007/s10967-024-09821-y.

Funding Open Access funding enabled and organized by Projekt DEAL.

Declarations

Conflict of interest The authors have no competing interests to declare that are relevant to the content of this article. The authors have no affiliations with or involvement in any organization or entity with any financial interest or non-financial interest in the subject matter or materials discussed in this manuscript. Data sets generated during the current study are available from the corresponding author on reasonable request. The 5th author, Zsolt Révay is a member of the Editorial Board of the journal. Therefore, he did not take part in the review process in any capacity and the submission was handled by a different member of the editorial board.

References

1. Molnár GL (2004) Handbook of prompt gamma activation analysis with neutron beams. Kluwer Academic Publishers ISBN 1-4020-1304-3
2. Zs R, Firestone RB, Belgya T, Molnár GL (2004) Prompt Gamma-Ray Spectrum. In: Molnár GL (ed) Handbook of prompt gamma activation analysis with neutron beams. Kluwer Academic Publishers, Dordrecht, pp 173–364
3. Database for Prompt Gamma-ray Neutron Activation Analysis, International Atomic Energy Agency Nuclear Data Services https://www-nds.iaea.org/pgaa/
4. Chu SYF, Ekström LP, Firestone RB, WWW Table of Radioactive Isotopes, database version 1999-02-28. http://nucleardata.nuclear.lu.se/toi/
5. Demidov A, Govor L, Cherepantsev M, Ahmed S, Al-Najjar M, Al-Amili N, Al-Assafi N, Rammo N (1978) Atlas of gamma-ray spectra from the inelastic scattering of reactor fast neutrons. Atomizdat, Moscow
6. Ahmed MR, Shakarchi KHI, Al-Najjar SA, Al-Amili MA, Govor LI, Demidov AM (1974) Investigation of gamma-ray spectra from the inelastic scattering of reactor fast neutrons. Nucl Instrum Methods 117:533–539
7. Hurst AM, Bernstein LA, Kawano T, Lewis AM, Song K (2021) The Baghdad Atlas: a relational database of inelastic neutron scattering (n, n´γ) data. Nucl Instrum Meth A 995:165095
8. Bernstein L, Brown D, Basunia S, Hurst A, Kawano T, Kelley J, Kondev F, McCutchan E, Nesaraja C, Slaybaugh R, Sonzogni A (2015) Nuclear data needs and Capabilities for Applications, White paper LLNL Report LLNL-CONF-676585, http://bang.berkeley.edu/events/ndnca/whitepaper

9. Romano C, Ault T, Bernstein L, Bahran R, Talou P, Quiter B, Pozzi S, Devlin M, Burke J, Bredeweg T, McCutchan E, Stave S, Bailey T, Hogle S, Chapman C, Hurst A, Nelson N, Tovesson F, Hornback D (2018) Proceedings of the nuclear data roadmapping and enhancement workshop (NDREW) for nonproliferation, In: White paper ORNL/LTR-2018/510, https://www.nndc.bnl.gov/nndcscr/documents/ndrew/NDREWProc_FINAL.pdf
10. Bernstein L, Romano C, Brown D, Casperson R, Descalle MA, Devlin M, Pickett C, Rearden B, Vermeulen C (2019) Final report for the workshop for applied nuclear Data activities (WANDA), White Paper LLNL-PROC-769849
11. Rossbach M, Genreith C, Randriamalala T, Mauerhofer E, Révay Z, Kudejova P, Söllradl S, Belgya T, Szentmiklosi L, Firestone RB, Hurst AM, Bernstein L, Sleaford B, Escher JE (2015) TANDEM: a mutual cooperation effort for transactinide nuclear
12. Randriamalala TH, Rossbach M, Mauerhofer E, Zs R, Söllradl S, Wagner FM (2016) FaNGaS: a new instrument for (n, n´γ) reaction measurements at FRM II. Nucl Instrum Methods A 806:370–377
13. Hable A, Ramsl C, Jericha E, Böck H, Randriamalala TH, Rossbach M (2017) FaNGaS: Determination of integral fast fission cross sections (n, f) of ^{23}8U, ^{23}7Np, and ^{24}2Pu in a directed fission neutron beam at FRM II. Garching, J Radioanal Nucl Chem. https://doi.org/10.1007/s10967-017-5512-7
14. Ilic Z, Mauerhofer E, Stieghorst C, Zs R, Rossbach M, Randriamalala TH, Brückel T (2020) Prompt gamma rays induced by inelastic scattering of fission neutrons on iron. J Radioanal Nucl Chem 325:641–645
15. Mauerhofer E, Ilic Z, Stieghorst C, Zs R, Rossbach M, Li J, Randriamalala TH, Brückel T (2021) Prompt and delayed gamma rays induced by epithermal and fast neutrons with indium. J Radioanal Nucl Chem 331:535–546
16. Mauerhofer E, Ilic Z, Stieghorst C, Zs R, Vezhlev E, Ophoven N, Randriamalala TH, Brückel T (2022) Prompt gamma rays from fast neutron inelastic scattering on aluminum, titanium and copper. J Radioanal Nucl Chem 331:3987–4000
17. Ophoven N, Ilic Z, Mauerhofer E, Randriamalala TH, Vezhlev E, Stieghorst C, Zs R, Brückel T, Jolie J, Strub E (2022) Fast neutron induced gamma rays from (n, n'), (n, p) and (n, α) reactions on CaCO3. J Radioanal Nucl Chem 331:5729–5740
18. Ophoven N, Ilic Z, Mauerhofer E, Randriamalala TH, Vezhlev E, Stieghorst C, Zs R, Brückel T, Jolie J, Strub E (2023) Prompt gamma rays from fast neutron induced reactions on cerium and chlorine. J Radioanal Nucl Chem 332:3133–3145
19. Ophoven N, Ilic Z, Mauerhofer E, Randriamalala TH, Vezhlev E, Stieghorst C, Zs R, Brückel T, Jolie J, Strub E (2023) Prompt gamma rays of terbium induced by inelastic scattering of fission neutrons. J Radioanal Nucl Chem 333:1287–1300
20. Mauerhofer E, Ophoven N, Ilic Z, Stieghorst C, Révay Zs, Meleshenkovskii I, Randriamalala TH (2024) Gamma emission from interaction of fission neutrons on nickel and zirconium. J Radioanal Nucl Chem (accepted)
21. Sommer LB, Chemnitz T, Kampfer S, Bausenwein D, Beimler A, Kellermeier M, Schütz R, Wilkens JJ, Wagner FM (2023) A new multi leaf collimator for the fission neutron therapy facility at FRM II. Nucl Instrum Methods A 1057:168717
22. Zs R, Belgya T, Molnár GL (2005) Application of hypermet-PC in PGAA. J Radioanal Nucl Chem 265:261–265
23. NuDat 3.0 National Nuclear Data Center, Brookhaven National Laboratory https://www.nndc.bnl.gov/nudat3/
24. Tilley DR, Weller HR, Cheves CM (1993) Energy levels of light nuclei A = 16–17. Nucl Phys A 564:1–183
25. Tilley DR, Weller HR, Cheves CM, Chasteler RM (1995) Energy level of light nuclei A = 18–19. Nucl Phys A 595:1–170
26. Chen J, Cameron J, Singh B (2011) Nuclear data sheets for A = 35. Nucl Data Sheets 112:2715–2850
27. Cameron J, Chen J, Singh B, Nica N (2012) Nuclear data sheets for A = 37. Nucl Data Sheets 113:365–514
28. Ouellet C, Singh B (2011) Nuclear data sheets for A = 32. Nucl Data Sheets 112:2199–2355
29. Joshi PK, Singh B, Singh S, Jain AK (2016) Nuclear data sheets for A = 139. Nucl Data Sheets 138:1–292
30. Nica N (2023) Nuclear data sheets for A = 141. Nucl Data Sheets 187:1–354
31. Reilly D et al (1991) Passive nondestructive assay of nuclear materials https://www.nrc.gov/docs/ML0914/ML091470585.pdf
32. NIST XCOM: Photons Cross Sections Database, National Institute of Standards and Technology https://physics.nist.gov/PhysRefData/Xcom/html/xcom1.html
33. Berger MJ, Hubbell JH, Seltzer S, Chang J, Coursey JS, Sukumar R, Zucker DS (2009) XCOM: photon cross sections database. NIST Stand Ref Database 8:87–3597
34. Initial MCNP6 Release Overview MCNP6 Version 1.0, Los Alamos National Laboratory report LA-UR-13-22934
35. Goorley T et al (2017) Initial MCNP6 release overview. Nucl Technol 180:298–315
36. Brown DA et al (2018) ENDF/B-VIII.0: the 8th major release of the nuclear reaction data library with CIELO-project cross sections, new standards and thermal scattering data. Nucl Data Sheets 148:1–142
37. MacFarlane RE, Kahler AC (2010) Methods for processing ENDF/B-VII with NJOY. Nucl Data Sheets 111:2739–2890
38. MacFarlane R, Muir DW, Boicourt RM, Kahler AC, Conlin JL (2017) The NJOY Nuclear Data Processing System, Version 2016. https://doi.org/10.2172/1338791
39. Barzilov A, Womble P (2014) Study of Doppler broadening of gamma-ray spectra in 14-MeV neutron activation analysis. J Radioanal Nucl Chem 301:811–819
40. Catz AL, Amiel S (1967) Study of lifetimes of nuclear levels by Doppler broadening attenuation using a (Ge)Li gamma-ray spectrometer. Nucl Phys A 92:222–232
41. Scheck M, von Brentano P, Fransen C, Kneissl U, Kohlstall C, Linnemann A, Mücher D, Pietralla N, Pitz HH, Scholl C, Stedile F, Walter S, Werner V, Yates SW (2007) Dipole strength distributions of the stable odd-mass N = 82 isotones ^{139}La and ^{141}Pr. Phys Rev C 75:044313
42. Révay Z (2009) Determining elemental composition using prompt γ activation analysis. Anal Chem. https://doi.org/10.1021/ac9011705